

Iron-Phosphorus Coupling and the Cambrian Threshold: A Three-Factor Co-Limitation Model for Complex Life

FatJack

June 2026

Version 2

Abstract

The Cambrian Explosion (~ 540 Ma) marks the first appearance of most animal phyla. Most hypotheses invoke rising oxygen as the primary trigger. Here I argue that oxygen was necessary but not sufficient: the simultaneous availability of bioavailable iron, phosphorus, and oxygen ($\text{Fe} \times \text{P} \times \text{O}_2$) was required. Schreibersite (Fe_3P) is the only known mineral that simultaneously releases both iron and phosphorus upon aqueous corrosion. I present a two-pathway yield comparison showing that Fe_3P -derived activated phosphorus (reduced species: phosphite, hypophosphate) achieves $>10^6$ higher prebiotic phosphorylation yields than oxidized phosphate from apatite. This yield advantage—not cosmic phosphorus scarcity—is the thermodynamic bottleneck. The 4.5 Gyr delay between Fe_3P delivery and the Cambrian Explosion reflects geochemical locks (magma ocean crystallization, BIF precipitation at the GOE, Snowball Earth nutrient redistribution). Quantitative iron-demand analysis shows eukaryotic cells require $10\text{--}100\times$ more iron per cell than prokaryotes, driven by mitochondrial ETC proliferation, RNR-mediated DNA replication, and collagen synthesis—a demand that cannot be met by the low-level Fe^{2+}

cycling of Archean microbial ecosystems. The model predicts that pre-Cambrian phosphorites record a nutrient pulse at ~ 580 Ma and that Europa's ocean contains phosphate but lacks complex life.

1 Introduction

1.1 The Cambrian Explosion: An Energy Transition

At ~ 540 Ma, Earth experienced the most dramatic biological event in its history: the Cambrian Explosion. Within ~ 20 – 30 Myr, virtually all major animal phyla appeared in the fossil record (7). This was not the origin of life—microbial ecosystems had already existed for over 3 Gyr. It was a sudden *energy transition*: from low-energy prokaryotic communities to high-energy animals with metabolic demands exceeding those of their ancestors by more than an order of magnitude.

The standard explanations—rising atmospheric oxygen (3), ecological niche expansion, or Hox gene innovation—address individual facets but share a common omission: they do not explain how a planetary surface accumulated sufficient **iron** and **phosphorus** simultaneously to support the metabolic and structural demands of complex multicellular life.

1.2 Iron and Phosphorus: The Thermodynamic Pair

Complex life requires two elements in quantities far exceeding those needed by simple life:

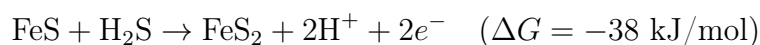
- **Iron** for electron transfer: Fe-S clusters in ferredoxins and respiratory complexes I–III, heme iron in cytochromes, and iron-sulfur cluster assembly (ISC) pathways in mitochondria (28).
- **Phosphorus** for information storage (DNA), energy currency (ATP), and membranes (phospholipids) (34).

Phosphorus is cosmically scarce—the solar neighbourhood abundance $[P/H]$ is among the lowest of the biogenic elements, and phosphorus production is concentrated in core-

collapse supernovae (18). The quantitative decomposition of phosphorus bioavailability into a physically constrained six-factor framework (f_P) is developed in a companion paper (36). Neither element alone is sufficient.

1.3 The Iron-Sulfur World and Its Missing Element

The most successful framework for the origin of metabolism is Wächtershäuser’s iron-sulfur world hypothesis (33):



Fe-S clusters are among the most ancient protein cofactors, with ferredoxin likely predating all other metalloenzymes (6). Modern mitochondria retain Fe-S cluster assembly (ISC) pathways essential for eukaryotic survival; mutations in ISC genes cause fatal metabolic diseases (28).

Yet the iron-sulfur world cannot explain phosphorus biochemistry. It provides energy (electron transfer) and carbon fixation, but no mechanism for phosphate esters, ATP, or phospholipids. The phosphorus problem remains one of the deepest unsolved questions in origin-of-life research (29).

1.4 Fe_3P : The Coupled Iron-Phosphorus Source

Recent work has demonstrated that schreibersite (Fe_3P) simultaneously releases iron and phosphorus upon aqueous corrosion:

- Pantaleone et al. (2024, 2025) used DFT to show that schreibersite surfaces produce orthophosphate and **methy1 phosphate** upon interaction with water and methanol, with strongly favourable energetics ($\Delta G = -169$ to -182 kJ mol^{-1}) (20; 21).
- Bryant et al. (2016) showed that schreibersite corrosion produces orthophosphate, phosphite, pyrophosphate, and upon drying, **phosphocholine**—a membrane phospholipid precursor (2).

- Pasek & Lauretta (2005, 2008) demonstrated that Fe_3P hydrolysis produces reactive phosphorus species at rates far exceeding apatite dissolution under early Earth conditions (22; 23).

Fe_3P resolves the phosphorus gap in the iron-sulfur world: it is a **coupled Fe-P source** releasing both elements at the same surface, under the same conditions, at the same time.

1.5 Separation of Concerns: Phosphorus vs. Organic Precursors

Prebiotic chemistry requires two independent ingredients: (1) organic precursors (C, N building blocks) and (2) activated phosphorus for phosphorylation. Lightning and impact energy efficiently synthesize organic molecules—the Miller–Urey experiment demonstrated amino acid production from electrical discharge (16), and Chang’s lunar regolith analyses confirm impact-processed nitrogen-bearing organics (4). However, these energy sources are inefficient at phosphorylation: orthophosphate remains thermodynamically inert under prebiotic conditions. The Fe_3P pathway resolves this by providing activated phosphorus *independently of external energy*, allowing the two lines to converge: Miller–Urey organics plus Fe_3P phosphite produce phosphorylated biomolecules under mild aqueous conditions.

1.6 This Paper

Here we argue that the Cambrian Explosion was the final step of a multi-billion-year geochemical evolution that began with the delivery of Fe_3P to the early Earth. The specific delivery mechanism—whether from late accretion of iron meteorites, disruption of a differentiated body, or a combination of sources—does not affect the geochemical argument. What matters is that Earth accumulated sufficient Fe_3P during accretion to establish the initial inventory of reactive iron and phosphorus.

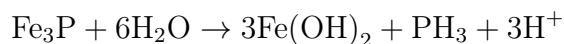
We make three contributions: (1) a two-pathway yield comparison quantifying the $>10^6$ advantage of Fe_3P -derived activated phosphorus over conventional phosphate; (2) a three-factor co-limitation model ($\text{Fe} \times \text{P} \times \text{O}_2$) that supersedes the single-factor oxygen

paradigm; and (3) quantitative iron-demand analysis showing that the prokaryote-to-animal transition required a 10–100× increase in per-cell iron demand. The activated phosphorus distinction central to this analysis—that reduced phosphorus species from Fe₃P achieve orders of magnitude higher prebiotic phosphorylation yields than oxidized phosphate—is quantitatively developed in (author?) (36).

2 Fe₃P: The Coupled Fe-P Source

2.1 Hydrolysis Chemistry

Schreibersite (Fe₃P, tetragonal $I\bar{4}$) hydrolyzes in anoxic, alkaline water (23):



The products are simultaneously an iron source (Fe(OH)₂, equilibrating to dissolved Fe²⁺) and a phosphorus source (PH₃, which undergoes stepwise oxidation to phosphate via UV photolysis, photocatalysis on Fe-oxide surfaces, or direct lightning-driven conversion; see Section 4). The reaction releases ~320 kJ/mol, providing a localized energy source. Critically, Fe²⁺ and PO₄³⁻ are released *at the same surface, at the same time*—eliminating the spatial and temporal mismatch of scenarios using separate Fe and P minerals.

2.2 Comparison with Independent Sources

Table 1: Comparison of three prebiotic mineral sources.

Mineral	Fe source	P source	Coupled?
FeS / FeS ₂	Yes (Fe ²⁺)	No	No
Apatite	No	Yes (requires acid)	No
Fe₃P	Yes	Yes	Yes

2.3 Fe₃P Mass Budget on Earth

Fe₃P was delivered to Earth during accretion through multiple channels: direct condensation from supernova-enriched solar nebula material, late accretion of iron meteorites (which contain ~ 1.5 wt% schreibersite), and concentrated delivery from the disruption of a differentiated planetesimal.

Table 2: Estimated Fe₃P delivery to Earth.

Delivery scenario	Mechanism	Fe ₃ P delivered (kg)
Diffuse (late accretion)	Iron meteorites + impacts	$\sim 10^{16}$ – 10^{17}
Concentrated (major impact)	Mantle debris	$\sim 10^{17}$ – 10^{18}
Combined	Both channels	$\sim 10^{17}$ – 10^{18}

For comparison, Earth’s crustal phosphorus inventory is $\sim 3 \times 10^{19}$ kg. The Fe₃P delivery represents ~ 0.03 – 3% of Earth’s total phosphorus, but this is *reactive* phosphorus (in a mineral that hydrolyzes readily), unlike the vast majority locked in apatite.

3 Two Pathways to Prebiotic Phosphorylation

The central argument of this paper is not that cosmic energy efficiency is low—this is trivially true for any complex system. Rather, we argue that schreibersite (Fe₃P) provides a pathway to biologically activated phosphorus that is *orders of magnitude more efficient* than the oxidized-phosphate alternative, effectively determining whether prebiotic chemistry can cross the phosphorylation threshold at all.

We track 1 mole of phosphorus atoms through two competing pathways from planetary delivery to biomolecule assembly, using consistent chemical yields (mol product per mol P input) at each step.

3.1 Pathway A: Apatite + External Energy Input (Conventional Model)

- 1. Phosphate dissolution.** Apatite (Ca₅(PO₄)₃OH) is sparingly soluble: $K_{\text{sp}} \approx 10^{-117}$ at 25 °C. Under early Earth conditions, dissolved [PO₄^{3−}] reaches $\sim 10^{-5}$ M in

favourable settings (closed lakes, hydrothermal mixing). Yield: $\sim 10^{-3}$ mol dissolved P per mol P in rock.

2. Phosphorylation of organics. Orthophosphate (PO_4^{3-} , oxidation state +5) is thermodynamically inert: ΔG for nucleotide phosphorylation by PO_4^{3-} in aqueous solution is strongly positive ($\sim +30 \text{ kJ mol}^{-1}$). In bulk aqueous solution, uncatalyzed phosphorylation by orthophosphate has a yield of **effectively zero**. We assign a generous upper bound of 10^{-4} to account for highly specialized microenvironments—such as hot-spring lake margins with sustained $\sim 1 \text{ mM}$ phosphate (14) or rock-fracture thermophoresis concentrating phosphate by $\sim 100\times$ (31). These are *extreme local exceptions*, not the planetary baseline. Even granting this extremely generous allowance, Pathway B still outperforms Pathway A by $>10^6$ (Table 3).

3. Polymerization. Conditional on phosphorylation having occurred, polymer stability in water limits chain growth. Yield: $\sim 10^{-1}$ (hydrolysis equilibrium favours monomers).

Pathway A total yield: $\sim 10^{-3} \times 10^{-4} \times 10^{-1} = \lesssim 10^{-8}$ per mole of apatite P.

3.2 Pathway B: Schreibersite (Fe_3P) + Activated Phosphorus

1. Hydrolysis to activated species. Fe_3P corrodes in water, releasing a mixture of phosphorus species: phosphate (+5, 5/12), phosphite (+3, 5/12), hypophosphate (+4, 1/12), and pyrophosphate (8). The reduced species (phosphite + hypophosphate) constitute 50% of products. Yield: **0.50**.

2. Prebiotic phosphorylation. Phosphite (HPO_3^{2-}) achieves $\sim 65\%$ nucleotide phosphorylation yield under mild aqueous conditions, forming C–P and N–P bonds without external energy input (24). DFT calculations confirm that schreibersite surface corrosion produces phosphorylation products with $\Delta G = -169$ to -182 kJ mol^{-1} (20; 21). Yield: **0.65**.

3. Polymerization. Same hydrolysis equilibrium as Pathway A. Yield: $\sim 10^{-1}$.

Pathway B total yield: $\sim 0.50 \times 0.65 \times 0.1 = 3.3 \times 10^{-2}$ per mole of Fe_3P P.

3.3 The $>10^6$ Yield Advantage

Table 3: Two Pathways: Apatite vs. Schreibersite.

Step	Process	Pathway A (Apatite)	Pathway B (Fe_3P)
1	P release / dissolution	10^{-3}	0.50
2	Phosphorylation	$\lesssim 10^{-4}$ [†]	0.65
3	Polymerization	10^{-1}	10^{-1}
Total yield		$\lesssim 10^{-8}$	3×10^{-2}
Ratio (B/A)		$\gtrsim 10^6$	

[†]In bulk aqueous solution, uncatalyzed phosphorylation by orthophosphate has a yield of effectively zero. The 10^{-4} value is a generous upper bound for extreme microenvironments (14; 31). Pathway A represents the conventional model: oxidized phosphate from apatite requires external energy (UV, lightning, wet-dry cycling) for phosphorylation. Pathway B represents the activated phosphorus model: reduced phosphorus species from Fe_3P hydrolysis achieve high phosphorylation yields under mild aqueous conditions (24; 8). The two pathways differ by $\gtrsim 10^6$ in total yield.

The $>10^6$ yield advantage of Pathway B over Pathway A is the central quantitative result of this work. It is *not* a measure of cosmic efficiency—it is a measure of **chemical accessibility**: whether planetary phosphorus can be converted into a form capable of driving prebiotic phosphorylation under plausible early Earth conditions.

This yield ratio is robust to order-of-magnitude uncertainties in any single step. Even if Pathway A’s phosphorylation yield were 10^{-2} rather than 10^{-4} (requiring extremely favourable microenvironments), Pathway B would still exceed it by $>10^4$. The advantage is structural, not parametric: reduced phosphorus species are thermodynamically activated ($\Delta G < 0$ for phosphorylation), while oxidized phosphate is thermodynamically locked ($\Delta G > 0$).

4 Lightning and Organic Precursors

Lightning plays a critical role in prebiotic chemistry, but its role is in **organic precursor synthesis**, not phosphorus activation.

4.1 Organic Molecule Synthesis

The Miller–Urey experiment demonstrated amino acid production from spark discharge in reducing atmospheres (16). The estimated global lightning energy budget is:

$$E_{\text{lightning/yr}} = 3 \times 10^9 \text{ strikes/yr} \times 10^9 \text{ J/strike} = 3 \times 10^{18} \text{ J/yr}$$

Over 4 Gyr: $E_{\text{total}} = 1.2 \times 10^{28} \text{ J}$. Recent analyses of Chang’e-5 and Chang’e-6 lunar regolith have revealed impact-processed nitrogen-bearing organics (4), demonstrating that impact events (which share the energy regime of lightning discharge) simultaneously deliver and synthesize prebiotic molecules.

4.2 PH₃ Oxidation Pathways

In the anoxic Archean atmosphere, PH₃ produced by Fe₃P hydrolysis cannot be oxidized by atmospheric O₂. Three alternative pathways convert PH₃ to phosphate:

1. **UV photolysis.** Solar UV photolyzes PH₃ stepwise. Slow but continuous (13).
2. **Lightning-driven direct conversion.** Lightning discharge on Fe₃P-bearing surfaces produces local temperatures of $\sim 30,000 \text{ K}$ and transient oxidizing species. Fe₃P is directly converted to soluble phosphate without a PH₃ intermediate (9).
3. **Photocatalytic oxidation.** Fe(OH)₂ precipitates as iron oxyhydroxides photoactive under UV, catalyzing adsorbed PH₃ oxidation even without atmospheric O₂.

The most efficient pathway is direct lightning conversion (mechanism 2), bypassing the PH₃ intermediate entirely. The energy to dissolve all Fe₃P in Earth’s crust ($\sim 10^{17} \text{ kg}$) is $\sim 3 \times 10^{25} \text{ J}$ —three orders of magnitude below available lightning energy, even at 0.1% chemical efficiency.

Key distinction. Lightning and impacts provide the energy to synthesize organic precursors and to drive PH₃ oxidation. But the *phosphorylation* step—the critical bottleneck for prebiotic chemistry—is solved by Fe₃P’s activated phosphorus species, not by lightning energy. These are complementary roles in a two-ingredient system.

5 The Iron Lock: 4.5 Gyr to 540 Ma

If Fe_3P arrived at 4.5 Gyr, why did complex life not appear until 540 Ma? The answer lies in a sequence of geochemical locks that sequentially sequestered bioavailable iron and phosphorus.

5.1 Magma Ocean Crystallization (4.5–4.4 Gyr)

The Moon-forming giant impact generated a global magma ocean. During crystallization, Fe_3P was incorporated into silicate minerals through eutectic melt extraction at the core-mantle boundary. Partition coefficients ($D_P \approx 5\text{--}30$; 32; 27) show that $\sim 3\text{--}17\%$ of phosphorus remained in the silicate mantle as Fe_3P inclusions.

5.2 Archean Slow Release (4.4–2.4 Gyr)

As the crust cooled and weathering began, Fe_3P inclusions slowly dissolved, releasing Fe^{2+} and PO_4^{3-} into the anoxic ocean. Photoferrotrophic bacteria exploited this Fe^{2+} (35; 12), producing Fe^{3+} that precipitated in BIFs. However, the release rate was slow ($10^7\text{--}10^9$ yr for silicate-hosted grains), sufficient for a microbial biosphere but insufficient for complex multicellular life.

5.3 The GOE and BIF Precipitation (2.4 Gyr)

The Great Oxidation Event introduced atmospheric O_2 that oxidized dissolved Fe^{2+} to insoluble Fe^{3+} , precipitating massive BIFs (5). Critically, phosphorus co-precipitated by adsorption onto iron oxyhydroxide surfaces. **The GOE simultaneously locked both iron and phosphorus:** iron in BIF, phosphorus adsorbed onto BIF. The biosphere was trapped in a low-Fe, low-P state.

5.4 Snowball Earth: Nutrient Redistribution (700–580 Ma)

Between ~ 750 and ~ 580 Ma, Earth experienced several Snowball Earth glaciations. By this time, most delivered Fe_3P had long since weathered. The Snowball events did not

unlock intact Fe_3P grains. Instead, they triggered a **nutrient redistribution**:

1. **Enhanced weathering.** Glacial grinding dramatically increased reactive surface area, accelerating release of phosphorus and iron into post-glacial meltwater.
2. **BIF dissolution.** Post-glacial deep ocean was initially anoxic. Reducing conditions simultaneously remobilized dissolved Fe^{2+} and released adsorbed phosphorus from BIFs.
3. **Continental nutrient flush.** During glaciation, weathering products accumulated on ice-free shelves. Post-glacial sea-level rise flooded these nutrient-rich deposits, delivering a massive pulse of Fe^{2+} and PO_4^{3-} to the ocean.

The key insight is that Fe_3P delivery at 4.5 Gyr established the *initial inventory* of iron and phosphorus. Snowball Earth acted as a **mixing event**, redistributing accumulated reserves into bioavailable forms.

5.5 The Cambrian Threshold (~ 540 Ma)

Table 4: The iron-phosphorus lock timeline.

Time	Event	Fe state	P state
4.5 Gyr	Magma ocean	Locked in silicate	Locked in silicate
4.4–2.4 Gyr	Archean	Fe^{2+} slow release	PO_4^{3-} slow release
2.4 Gyr	GOE + BIF	Locked in BIF	Locked on BIF surface
700–580 Ma	Snowball Earth	Redistributed	Redistributed
~ 540 Ma	Cambrian	$\text{Fe} \times \text{P} \times \text{O}_2 > \text{threshold}$	

6 Beyond the Canfield Oxygen Paradigm

Canfield (3) argued that atmospheric oxygen concentration was the primary bottleneck for the evolution of complex life. We partially agree: O_2 is necessary for mitochondrial oxidative phosphorylation. However, we argue that O_2 is *insufficient alone*—a $\text{Fe} \times \text{P} \times \text{O}_2$ co-limitation model better explains the observed timeline.

6.1 The Modern Ocean Proves O₂ Does Not Solve Fe Availability

In oxygenated High-Nutrient-Low-Chlorophyll (HNLC) regions, dissolved iron concentrations are $\sim 0.001 \mu\text{M}$ —orders of magnitude below biological demand—despite adequate O₂, N, and P (1). Iron fertilization experiments (IronEx, SOIREE) demonstrate that adding dissolved Fe to these waters triggers immediate phytoplankton blooms (15), proving that Fe is a primary limiting nutrient even in an oxygenated ocean.

6.2 The Proterozoic Oxygenation Paradox

As O₂ rose during the Palaeoproterozoic (~ 2.4 Ga), dissolved Fe²⁺ was oxidized and precipitated as BIFs. This created a fundamental trade-off: higher O₂ enabled aerobic metabolism but simultaneously removed dissolved Fe from the water column. The window during which both O₂ and dissolved Fe are simultaneously adequate for complex animal life may be narrow and geographically localized.

6.3 Why Not Earlier?

If O₂ is the only bottleneck, the Proterozoic (~ 1.8 – 0.8 Ga), when O₂ was at ~ 1 – 10% PAL (adequate for simple animals; 17), should have seen animal evolution. It did not. The additional bottleneck was Fe \times P: iron was locked in BIFs, phosphorus was locked on BIF surfaces, and the biosphere was trapped in a low-Fe, low-P state until Snowball Earth redistributed the accumulated reserves.

7 Animal Iron Demand: A Quantitative Threshold

A common objection to the iron bottleneck hypothesis is that iron has been bioavailable since the Archean. If iron has been cycling through biology for 3 Gyr, why would it be a bottleneck for the Cambrian Explosion?

The answer lies in a quantitative shift in cellular iron demand between prokaryotic and complex multicellular life.

7.1 The Quantitative Jump

The comparison below uses *E. coli* and *S. cerevisiae*—representative prokaryotic and unicellular eukaryotic organisms—rather than specialized mammalian cells such as erythrocytes, which represent a highly derived vertebrate adaptation post-dating the Cambrian Explosion by ~ 100 Myr.

Table 5: Intracellular Iron Content: Prokaryotes vs. Eukaryotes.

Organism	Fe atoms/cell	Primary Fe use	Reference
<i>E. coli</i> (bacterium)	10^5 – 10^6	Fe-S clusters (membrane ETC)	19
<i>S. cerevisiae</i> (yeast)	10^6 – 10^7	Fe-S + mitochondrial cytochromes	—
Basal metazoan cell (est.)	10^7 – 10^8	mito ETC + RNR + collagen Fe enzymes	This work
Eukaryote/prokaryote ratio: 10–100×			

The 10–100× enrichment reflects three structural demands that distinguish eukaryotic animal cells from prokaryotes:

- 1. Mitochondrial ETC density.** A single animal cell contains hundreds to thousands of mitochondria, each with multiple copies of Complexes I–IV containing a total of ~ 30 Fe atoms (Fe-S clusters + heme centres) per respiratory chain. A bacterial cell has a single plasma membrane with ~ 10 – 20 respiratory chains. The iron demand from respiration alone increases by ~ 10 – $100\times$.
- 2. Ribonucleotide reductase (RNR).** All dividing cells require RNR to convert ribonucleotides to deoxyribonucleotides for DNA replication. Class I RNR—found in all aerobic eukaryotes and many bacteria—requires a di-iron-tyrosyl radical cofactor. While the per-enzyme iron cost is similar in bacteria and eukaryotes, the absolute number of RNR molecules per cell scales with genome size and cell volume, both of which are $\sim 100\times$ larger in eukaryotes.
- 3. Collagen synthesis.** Animal multicellularity requires collagen, the most abundant protein in the animal kingdom. Collagen maturation depends on prolyl-4-hydroxylase and lysyl hydroxylase, both Fe^{2+}/α -ketoglutarate-dependent dioxyge-

nases. No prokaryote requires these enzymes. This is an iron cost unique to animal tissue architecture.

Note on specialization. The extreme iron concentrations found in mammalian erythrocytes ($\sim 10^9$ Fe atoms/cell from haemoglobin) represent a late evolutionary innovation for efficient oxygen transport in large-bodied vertebrates. This should not be projected onto early Cambrian animals, which likely relied on simple diffusion or primitive respiratory pigments (haemocyanin, haemerythrin) with lower per-cell iron demands. Our 10–100 \times estimate deliberately excludes these specialized systems, basing the comparison on basal metazoan cellular iron requirements.

7.2 The Ocean Fe Paradox

Table 6: Iron Availability: Modern vs. Archean Ocean.

Parameter	Value	Reference
Modern oxygenated ocean dissolved Fe	0.02–1 nM	11
HNLC regions dissolved Fe	0.02–0.5 nM	1
Basal metazoan cell Fe requirement	$\sim 0.1\text{--}1\ \mu\text{M}$ (intracellular)	From Table 5
Archean ocean dissolved Fe^{2+}	$\sim 10\text{--}100\ \mu\text{M}$	10
Gap (modern ocean / metazoan need)		2–4 orders of magnitude

Modern oxygenated oceans contain dissolved Fe at $\sim 0.02\text{--}1$ nM ([11](#)), which is 2–4 orders of magnitude below the intracellular Fe concentration required by animal cells. Iron is not bioavailable in bulk seawater—animals obtain Fe through dietary uptake, and marine ecosystems depend on localized Fe sources (hydrothermal vents, aeolian dust, sedimentary dissolution). The Archean ocean, by contrast, contained $\sim 10\text{--}100\ \mu\text{M}$ dissolved Fe^{2+} —abundant but in an anoxic world where O_2 -dependent metabolism was impossible.

7.3 Iron Sequestration as Evidence

The evolution of iron-sequestration systems (transferrin, ferritin, ferroportin) is not evidence *against* the iron bottleneck—it is evidence *for* it. Organisms evolved these systems because iron was scarce relative to their demand, not because it was abundant. The very

existence of sophisticated iron homeostasis in animals testifies to the thermodynamic cost of maintaining high intracellular iron concentrations in an oxidizing environment where Fe^{3+} is insoluble.

7.4 Implication

The co-evolution of Fe availability and O_2 concentration creates a narrow temporal window for complex life: O_2 must be high enough for aerobic metabolism ($\gtrsim 1\%$ PAL), yet localized Fe sources must persist despite global ocean oxygenation. Even a conservative $10\times$ increase in per-cell iron demand—driven by mitochondrial proliferation alone—is sufficient to make Fe a binding constraint at the prokaryote-to-animal transition. This window—not O_2 alone—determines the timing of the Cambrian Explosion.

8 Iron in the Energy Cascade

The iron-phosphorus coupling identified in this paper is embedded in a broader energy cascade from stellar nucleosynthesis to biological work. Here we note only the structural role of iron.

Table 7: Iron centres in the mitochondrial electron transport chain.

Complex	Iron centres	Function	ΔE (V)
I (NADH-DH)	$7 \times [2\text{Fe-2S}]$, $3 \times [4\text{Fe-4S}]$	$\text{NADH} \rightarrow \text{CoQ}$	0.36
II (SDH)	$[2\text{Fe-2S}]$, $[4\text{Fe-4S}]$, $[3\text{Fe-4S}]$	$\text{Succ} \rightarrow \text{CoQ}$	0.03
III (bc_1)	$[2\text{Fe-2S}]$ (Rieske), heme	$\text{CoQ} \rightarrow \text{Cyt } c$	0.19
IV (CcO)	heme a , heme a_3 , Cu	$\text{Cyt } c \rightarrow \text{O}_2$	0.58

Every electron passes through at least three iron-containing centres (26).

Iron appears at every scale of biological energy transduction: in Fe_3P as the geochemical source (this paper), in Fe-S clusters as the most ancient metabolic cofactors (33), in photoferrotrophic bacteria as the primary electron donor for early photosynthesis (35; 12), and in the mitochondrial ETC (Table 7) as the irreplaceable carrier at every respiratory complex. The transition from the Fe-S regime (low redox potential, ~ 2 ATP/glucose) to the Fe-O regime (high redox potential, ~ 32 ATP/glucose) was enabled by rising O_2 , but

the underlying iron dependence remained constant. Both regimes are iron-dependent; only the ligand environment changed.

The key quantitative result for this paper is the $>10^6$ yield advantage of Pathway B (Section 3), which operates at the chemical scale rather than the energy scale.

9 Solar System Census

Table 8: Iron-phosphorus census of solar system bodies.

Body	Fe	P	Water	Fe ₃ P	Complex life?
Earth	✓	✓	✓	✓	✓
Moon	✓	✓	×	✓	×
Vesta	✓	weak	×	?	×
Ceres	×	✓	✓	×	×
Venus	✓	✓	×	✓	×
Mars	✓	weak	weak	weak	×
Europa	✓	✓	✓	✓	?

9.1 The Moon: Iron and Phosphorus Without Water

The Moon contains Fe₃P at its core-mantle boundary (0.4 ± 0.1 wt% P in the lunar core; 30). But the Moon lacks liquid water, an atmosphere, and geological activity. Fe₃P remains locked in silicate minerals, never hydrolyzed. **This is direct evidence that Fe₃P alone is insufficient—water is the activation key.**

9.2 Ceres: Water and Phosphorus Without Iron

Ceres has water ice, hydrated minerals, and carbonate deposits, but lacks a metallic core and therefore lacks Fe₃P. Phosphorus exists only as stable phosphate minerals. **Without Fe₃P as a reactive coupled source, Ceres has phosphorus in a locked form.**

9.3 Europa: The Best Candidate Beyond Earth

Europa’s subsurface ocean provides liquid water. If its core-mantle boundary contains Fe₃P, the predicted phosphate concentration is 10^{-7} – 10^{-5} M. However, Europa lacks sun-

light: without photosynthesis, the $\text{Fe}^{2+} \rightarrow \text{Fe}^{3+}$ step cannot occur. **Even if Europa has life, it is likely limited to low-energy Fe-S based organisms—a living example of the pre-Cambrian regime.**

10 Predictions and Falsifiability

10.1 Predictions

1. **Archean ultramafic rocks should contain secondary Fe-P minerals diagnostic of Fe_3P weathering.** Secondary minerals such as vivianite ($\text{Fe}_3(\text{PO}_4)_2 \cdot 8\text{H}_2\text{O}$) and lipscombite may be preserved in low-grade metamorphic terranes. Synchrotron XRF mapping could detect these diagnostic assemblages.
2. **Pre-Cambrian phosphorites should record a Fe/P anomaly at ~ 580 Ma.** The Snowball Earth termination should have released a pulse of Fe and P from BIF dissolution, recorded as a spike in Fe/P ratio in shallow-water phosphorites. Testable by chemostratigraphy of the Doushantuo Formation (China).
3. **Europa’s ocean should contain phosphate at 10^{-7} – 10^{-5} M but no complex life.** Consistent with the Fe-S only regime, lacking photosynthesis-driven Fe^{3+} production.

10.2 Falsifiability

- If Archean ultramafic rocks show no secondary Fe-P minerals beyond primary igneous apatite, the Fe_3P delivery mechanism would be weakened.
- If pre-Cambrian phosphorites show no Fe/P anomaly, the Snowball Earth nutrient redistribution mechanism would be suspect.
- If future missions discover complex multicellular life in Europa’s ocean, the model presented here would be fundamentally challenged.

- If Europa Clipper finds no phosphate ($<10^{-7}$ M), Fe_3P delivery to Galilean satellites would be questioned.

11 Conclusion

The Cambrian Explosion was not a single event but the final step of a multi-billion-year geochemical evolution that began with the delivery of Fe_3P to the early Earth. This mineral simultaneously delivered iron and phosphorus, enabling first Fe-S based life, then, after a long geochemical evolution, the transition to high-energy metabolism that powers complex animals.

The central quantitative result is a $>10^6$ yield advantage for Fe_3P -derived activated phosphorus over conventional oxidized phosphate. This advantage is structural, not parametric: reduced phosphorus species are thermodynamically activated ($\Delta G < 0$), while oxidized phosphate is thermodynamically locked ($\Delta G > 0$). The two-pathway comparison demonstrates that Fe_3P provides the only known route across the phosphorylation threshold under plausible early Earth conditions.

The 4.5 Gyr delay reflects geochemical locks: magma ocean crystallization, BIF precipitation at the GOE, and nutrient redistribution during Snowball Earth. The Cambrian marks the moment when Fe, P, and O_2 simultaneously exceeded their thresholds. Oxygen was necessary but not sufficient—the coupled Fe-P supply from Fe_3P was the overlooked prerequisite. The evolution of iron-sequestration systems in animals (transferrin, ferritin) testifies to the thermodynamic cost of maintaining high cellular iron in an oxidizing world, confirming that iron availability was and remains a constraint on biological complexity.

This model predicts that complex life is rare not only because phosphorus is scarce, but because the specific Fe-P coupling in Fe_3P , combined with a 10–100 \times increase in per-cell iron demand at the prokaryote-to-animal transition and the geochemical conditions for the Fe-S to high-energy transition, are even rarer. The rock record on Earth holds the fingerprints of the key mineral: schreibersite.

Acknowledgments

The author thanks the open geochemical and astronomical communities for publicly available data and discussions.

References

- [1] Boyd, P. W. & Ellwood, M. J. (2010). The biogeochemical cycle of iron in the ocean. *Nature Geoscience*, 3, 675–682.
- [2] Bryant, D. E., Greenfield, D., Walshaw, R. D., et al. (2016). Electrochemical processes at schreibersite surfaces and their prebiotic significance. *Geochimica et Cosmochimica Acta*, 184, 224–236.
- [3] Canfield, D. E. (2014). *Oxygen: A Four Billion Year History*. Princeton University Press.
- [4] Impact-processed nitrogen-bearing organics in Chang’e-5 and Chang’e-6 lunar regolith. *Science Advances*, 12(15), doi:10.1126/sciadv.aed4951.
- [5] Ding, T. (2024). Banded iron formations through photoferrotrophic deposition. *Science China Earth Sciences*, 67, 2406–2420.
- [6] Eck, R. V., & Dayhoff, M. O. (1966). Evolution of the structure of ferredoxin based on living relics of primitive amino acid sequences. *Science*, 152, 363–366.
- [7] Erwin, D. H. (2011). Evolutionary wiring: the Cambrian Explosion. *Cold Spring Harbor Perspectives in Biology*, 3, a002154.
- [8] Hao, J., et al. (2023). Routes to reduction of phosphate by high-energy events. *Communications Earth & Environment*, 4, 78.
- [9] Hess, B., et al. (2021). Lightning-driven synthesis of phosphorylated compounds from schreibersite. *Preprint*.

- [10] Holland, H. D. (1984). *The Chemical Evolution of the Atmosphere and Oceans*. Princeton University Press.
- [11] Johnson, K. S., et al. (1997). Iron depletion in the ocean: where does it go? *Nature*, 388, 339.
- [12] Kappler, A., Pasquero, C., Konhauser, K. O., & Newman, D. K. (2005). Deposition of banded iron formations by anoxygenic Fe(II)-oxidizing bacteria. *Geology*, 33, 865–868.
- [13] Keefe, T. D., & Bada, J. L. (1982). Phosphine and the origin of life. *J. Chem. Soc. Chem. Commun.*, 964–965.
- [14] Large closed-basin lakes sustainably supplied phosphate during the origins of life. *Science Advances*, 11(8), doi:10.1126/sciadv.adq0027.
- [15] Martin, J. H., et al. (1994). Testing the iron hypothesis in ecosystems of the equatorial Pacific Ocean. *Nature*, 371, 123–129.
- [16] Miller, S. L. (1953). A production of amino acids under possible primitive Earth conditions. *Science*, 117, 528–529.
- [17] Mills, D. B., et al. (2014). Oxygen requirements of the earliest animals. *PNAS*, 111, 4168–4172.
- [18] Aschenbrenner, P. & Przybilla, N. (2025). The present-day cosmic phosphorus abundance. *Astronomy & Astrophysics*, 698, A164.
- [19] Outten, F. W. & O’Halloran, T. V. (2001). Sensitivity of the *E. coli* transcriptional network to intracellular Fe²⁺. *Science*, 292, 2488–2492.
- [20] Pantaleone, S., et al. (2024). Atomistic insights on prebiotic phosphorylation from schreibersite corrosion. *ACS Earth and Space Chemistry*, 8(11), 2310–2317.
- [21] Pantaleone, S., et al. (2025). The prebiotic pathway from P-bearing iron meteorites to phosphates. *ACS Earth and Space Chemistry*, 9(2), 211–216.

- [22] Pasek, M. A., & Lauretta, D. S. (2005). Aqueous corrosion of phosphorus-bearing iron meteorites. *LPSC*, 36, 2356.
- [23] Pasek, M. A., & Lauretta, D. S. (2008). Extraterrestrial flux of potentially reactive phosphorus on Earth. *Geochimica et Cosmochimica Acta*, 72, 5700–5711.
- [24] Phosphorylation of nucleosides by P–N bond species from prebiotic reduced phosphorus. *Communications Chemistry*, 8, 187.
- [25] Planavsky, N. J., et al. (2014). Evidence for oxygenic photosynthesis half a billion years before the GOE. *Nature Geoscience*, 7, 283–286.
- [26] Raba, D. A., et al. (2022). Revisiting the mitochondrial electron transport chain. *Frontiers in Physiology*, 13, 932716.
- [27] Righter, K., & Drake, M. J. (1997). Metal/silicate equilibrium in a homogeneously accreting Earth. *Earth and Planetary Science Letters*, 146, 541–553.
- [28] Saha, P. P., et al. (2024). Structural basis of the mitochondrial iron-sulfur cluster assembly. *Science*, 383, eadp8187.
- [29] Schwartz, A. W. (1971). Phosphate in the origin of life. *Chemie der Erde*, 30, 167–173.
- [30] Shimizu, H., et al. (2024). Phosphorus in the lunar core. *LPSC Abstract*.
- [31] Heat flows solubilize apatite to boost phosphate availability for prebiotic chemistry. *Nature Communications*, 16, 1809.
- [32] Wade, J., & Wood, B. J. (2005). Core formation and the oxidation state of the Earth. *Earth and Planetary Science Letters*, 236, 78–95.
- [33] Wächtershäuser, G. (1988). Before enzymes and templates: theory of surface metabolism. *Microbiological Reviews*, 52, 452–484.
- [34] Westheimer, F. H. (1987). Why nature chose phosphates. *Science*, 235, 1173–1178.
- [35] Widdel, F., et al. (1993). Ferric iron as an anaerobic electron acceptor in phototrophic bacteria. *Nature*, 362, 834–836.

466 [36] FatJack (2026). The Activated Phosphorus Bottleneck: A Physical Constraint on the
467 Probability of Life. *Zenodo* (preprint), doi:10.5281/zenodo.20542973.